Chapter 16

Surface Modification of Polymer Materials Induced by Laser Irradiation

Rozalina Zakaria

Additional information is available at the end of the chapter

http://dx.doi.org/10.5772/66377

Abstract

We report on the surface modification effects using allyl-diglycol CR39 polymer induced by laser irradiation at 157 nm F_2 laser (VUV) and 248 nm KrF laser. The motivation is to investigate the ablation effects on this polymer in optical waveguides application the ablation effects on this polymer in optical waveguides. Fabrication of waveguides has been observed using continuous wave (CW) at 244 nm argon ion laser. Ablation effects on the surface of this polymer have been characterized including ablation threshold at different wavelengths from the assorted depth of craters formed from UV pulsed laser. Application of this polymer in optical waveguide application is corroborated by the refractive index value on the CR39 channels that varied as fluences changed when using the continuous wave UV irradiation. A limit for upper fluence at the point where laser ablation originates on this polymer has also been determined.

Keywords: CR39 laser ablation, surface modification, refractive index modification, channel waveguide

1. Introduction

Study of interaction of lasers with polymer materials that induce surface modification and ablation has been an interesting topic for decades [1]. Polymeric materials have been used in various applications such as high-performance photonics devices and engineering applications such as micro/nanofluidics channel fabrication, micromachining/microdrilling [2, 3], splitters, waveguide gratings and filters, and also in optical waveguide fabrication [3–5]. One of the most significance in the research field of photonics is refractive index modification of germanium-doped silica glass using 244 nm UV-laser irradiation as well as stud-

ies on nonlinear refractive index change of glass by femtosecond laser irradiation [6]. It has been reported through time regarding the interaction of polymer materials with laser at different photoetching techniques by means of infrared nanosecond laser, femtosecond laser as well as excimer laser [7]. Nevertheless, several parameters in combination including, among others, the material as well as the laser pulse and energy affect the material removing processes [8].

In this work, we focus on using F_2 (157 nm laser) and KrF (248 nm laser) to obtain ablation threshold for these materials at these wavelengths. Refractive index of CR39 is changed by varying the laser fluences using continuous wave laser. To obtain higher fluence in respect of the changes to be made, the laser spot size is focused down to microns in diameter.

For pulse laser, an aperture size of 6 × 3 mm is aligned and positioned in front of the lens to ensure substantial edge of craters can be seen on the film. Subsequently, examination of the pulse crater is carried out using a microscope to conclude the depth of each crater. After a few pulses, the correlation between adjustments of fluence and etch depth is determined. The exact number of pulses depends upon the fluence, wavelength, and absorption of the polymer in which the system will settle down to a constant etch depth per pulse. On the other hand, when continuous wave laser is used, the refractive index calculated after laser induced depends on the numerical aperture (NA) measurement on the written waveguides. Positive refractive index is perceived, and consequently, the association between irradiation fluence and refractive index change can then be concluded. In cases where laser ablation is initiated above this perimeter, an upper fluence limit could also be attained.

2. Experimental procedure

2.1. VUV F_2 laser

A 157 nm VUV F_2 laser (Lambda Physik LPF 200) that produced output energy of up to 35 mJ in an 11 ns pulse (full width at half maximum) was used to expose the various polymer samples. The charging voltage of the laser could be varied in 1 kV steps from 21 to 26 kV, and this allowed the laser energy and hence fluence at the target to be varied. The full-angle beam divergence of the direct output beam was ~3 mrad in its narrow dimension and ~8 mrad in its long dimension.

The polymer samples were held on a motorized stage, which was capable of movements in the *x-y-z* directions in increments from 1 mm to 1 cm under computer control. Due to the high absorption of the 157 nm wavelength in oxygen in air, the laser output had to be delivered either in vacuum or in a rare gas such as argon. In these experiments, the target was placed in a chamber that was capable of being evacuated down to 1×10^{-5} mbar. The chamber was evacuated using a dry pump, and the pressure was measured using Edwards Pirani/Penning 1005 pressure gauges. The chamber could also be purged with He or Ar gas as an alternative for beam delivery but in these experiments this was not used. **Figure 1** shows a schematic diagram of the F_2 laser experimental setup.

http://dx.doi.org/10.5772/66377

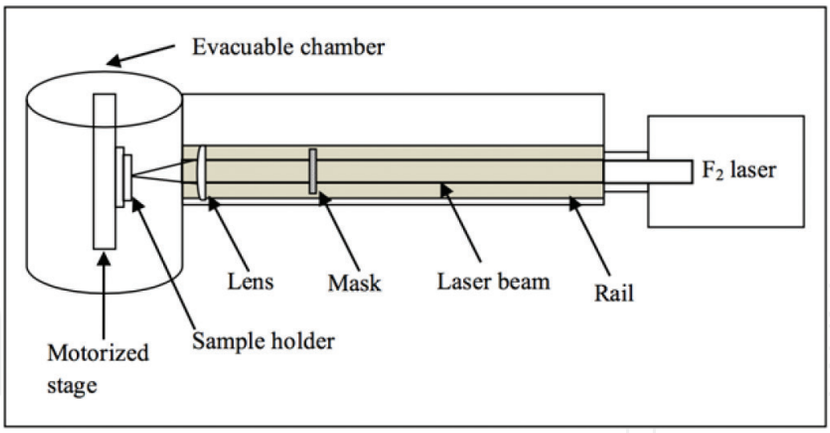

Figure 1. F_2 laser experimental setup.

2.2. 248 nm Pulsed UV laser

KrF excimer laser (Opto Systems Ltd Excimer Laser series CL5100) operating at 248 nm wavelength was the laser tools used in this research. The maximum repetition rate can range up to 100 Hz with a maximum average output power of 5 W and a pulse interval range from 9 to 11 ns. A 50 mm focusing lens is used to focus the light onto the CR39, which has a thickness of 1 mm and is in a sheet form (Solar lens product). A three-axis *x-y-z* translational platform was used to mount the sample. In the effort to position the polymer at the focus point, the sample location was varied through the micrometer-driven sample holder. The minimum spot size formed on the surface of the CR39 at the focus of the laser beam is noted as $465 \times 255\,\text{nm}^2$. Fluence of laser ablated on the CR39 can be calculated from the ratio of pulse energy (mJ) per laser spot area:

$$\text{Fluence} = \text{Energy}\,(\text{mJ}) / \text{Area}\,(\text{cm}^2) \tag{1}$$

For the whole experiments, fluence measurements are within an uncertainty of ±5%.

2.3. Continuous UV laser

For waveguide channel fabrication on CR39, a frequency-doubled argon ion laser emitting at 244 nm was used as a light source. The laser beam is focused by a 25-mm focusing lens onto the CR39. It was placed onto a three-axis stepper motor. By translating the stepper motor along the laser focusing plane, straight waveguides were produced. Fluence of laser irradiation on the CR39 can be calculated using the following equation [9]:

$$Fluence = P_{out}.d / v.A \tag{2}$$

where F is the fluence, P_{out} is the power of fiber output, d is the diameter of the beam, v is the relative traveling speed, and A is the area of the beam.

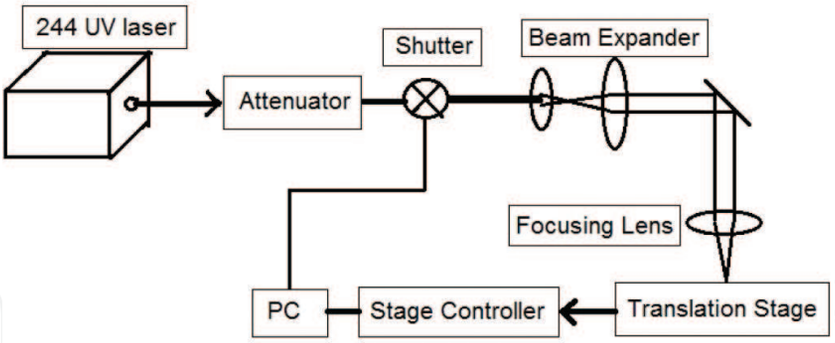

Figure 2. Waveguide channel written experimental arrangement.

The measured numerical aperture (NA) of the written waveguide can be used to compute the refractive index change, ΔRI of the UV irradiated area using the formula below:

$$NA = \left(n_c - n_{cl}\right)^{1/2} \tag{3}$$

where n_c and n_{cl} are the refractive index of UV written area and unwritten area, respectively. ΔRI can be calculated from the difference between n_c and n_{cl}.

A fiber pigtail was used to couple a tunable laser source into the CR39 waveguides to measure NA, whereas an objective lens was used to display the output of CR39 waveguides onto an image capture device. The formula below can be used to measure the NA of a waveguide from the waveguides divergence angle, θ:

$$NA = N_C \sin\theta \tag{4}$$

A straight waveguide with 3 cm length was fabricated using different fluences (between 1 and 5 KJ cm^{-2}). During this process, the laser power was set at a fixed value, and the laser beam was aligned to ensure that the focal plane was positioned on the CR39 sample surface. **Figure 2** shows the schematic diagram of waveguide channel written on the polymer.

3. Results and discussion

3.1. Etch rate analysis at 157 nm F_2 laser

Figure 3 shows a plot of the etch rate per pulse versus fluence for CR39 as derived from the white light interferometer; based on the linear fits for ≥10 pulse exposure, the estimated ablation threshold is ~60 mJ m^{-2}. However, **Figure 3** shows that there is still a small level of etching at a fluence of ~50 mJ cm^{-2}, and thus the estimated ablation threshold for CR39 is taken to lie in the range ~50–60 mJ cm^{-2}. From **Figure 3**, the etch rate per pulse for a single pulse reached ~100 nm at ~120 mJ cm^{-2}, higher than for multiple exposure. The data for 50 pulse exposure gave reasonably consistent values, and the gradient of the corresponding line in **Figure 3** gave an effective absorption coefficient of $\alpha_{eff} \approx 2.9 \times 10^5$ cm^{-1}. This is similar

http://dx.doi.org/10.5772/66377

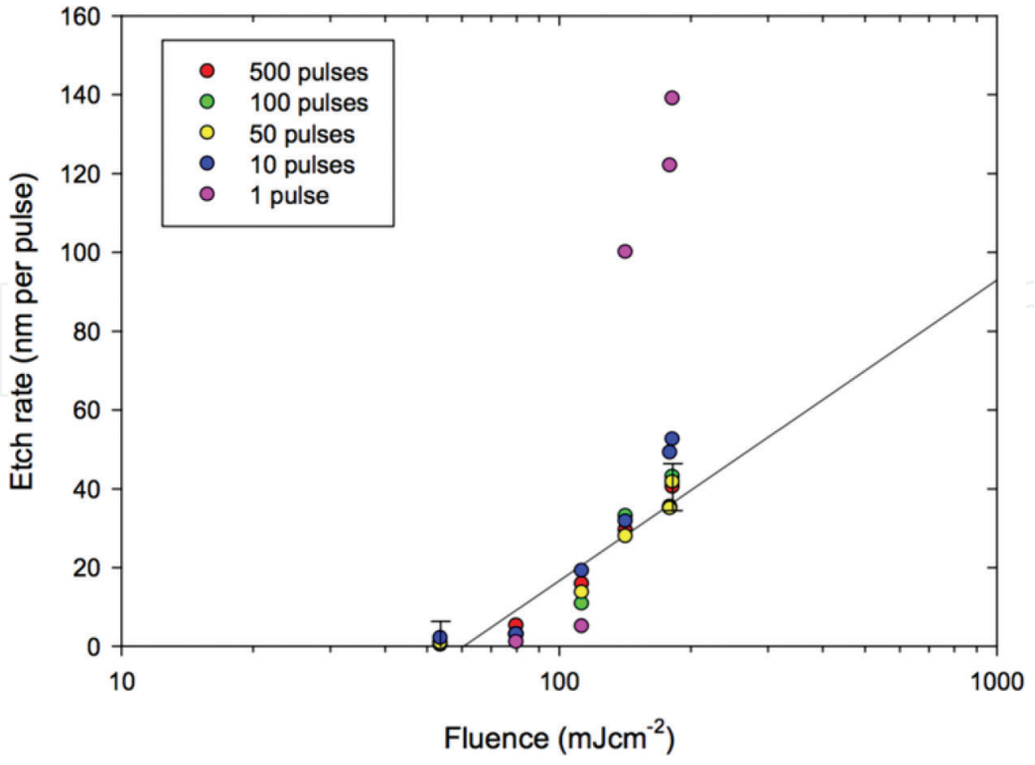

Figure 3. Etch rate as a function of fluence for CR39 polymer using the 157 nm laser. Results for the average etch rate per pulse for various numbers of pulses are shown.

to polycarbonate and indicates CR39 is a strongly absorbing organic polymer at 157 nm. No data relating to the optical constants in the VUV spectral region could be found for this material.

3.1.1. Formation of cones

For this experiment, clean CR39 samples (unseeded) were irradiated using 157 nm laser radiation over a range of pulse number from a single pulse to thousands of pulses and over a range of fluences of ~50 to ~180 mJ cm^{-2}. The dark spots that were seen under optical microscopy in the previous section were confirmed by scanning electron microscopy to be cones on the CR39 surface. These had very well-defined structures and, in general, appeared to have even better definition than those on the irradiated polycarbonate surface. In particular, the cones on CR39 were found to have extremely straight walls and to be exceptionally sharp at their tips as can be seen from the results shown in **Figure 4**. From the SEM images of the ablation sites, small particles appeared to be on the surface though it is difficult to make out if these reside on the top of the cone as "initiating" sites. **Figure 4a** and **b** shows the cones that developed at fluences of 112 and 180 mJ cm^{-2} with 500 pulses. The cones appear to have a similar size and shape at the same fluence. A comparison of **Figure 4a** and **b** shows as expected that the cone apex angle is larger at the lower fluence, that is, the full apex angle is ~70° at 112 mJ cm^{-2} and ~55° at 180 mJ cm^{-2} when corrected for the 60° viewing angle. It also appears that the cone tips get sharper as the fluence is raised. Exposure of the CR39 surface to a higher number of

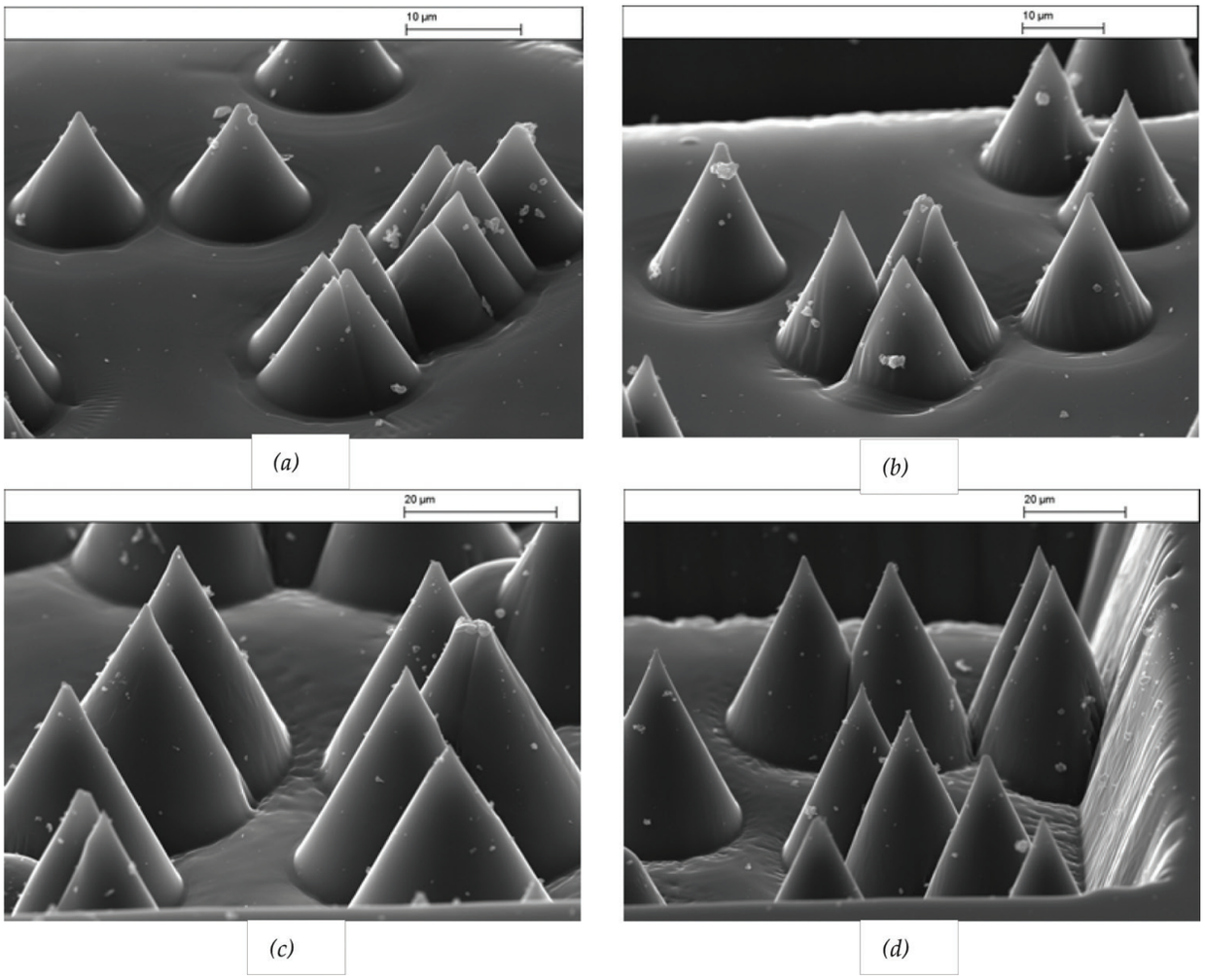

Figure 4. Examples of cone formation on the CR39 surface using the 157 nm laser (a) 500 pulses at 112 mJ cm^{-2} (b) 500 pulses at 180 mJ cm^{-2} (c) 1000 pulses at 142 mJ cm^{-2}, and (d) 1000 pulses at 182 mJ cm^{-2}.

pulses, **Figure 4c** and **d** led to an increase in the areal density of the cones compared to that at lower pulse number, **Figure 4a** and **b**.

Figure 5 shows a group of cones produced with 500 pulses at a fluence of ~80 mJ cm^{-2}. In this case, full apex angle of the cone is 83° corrected for the viewing angle of 60° on the SEM. At this fluence of ~80 mJ cm^{-2}, the cones have not fully developed and are not as well defined as those seen at higher fluences (**Figure 5b** and **c**), where the full apex angle is 66° and 51°, respectively, again illustrating that the angle is reduced at higher fluence. Here, they are fully developed, with sharp tips, and very well-defined structure.

In **Figure 5**, the ablated surface of this polymer well away from the cone bases is seen to be relatively smooth and devoid from significant debris indicating the good surface quality of this material when ablated with the 157 nm laser. The fringes around the bottom of the cones can be clearly seen in **Figure 6a** with 100 pulses at ~60 mJ cm^{-2} and **Figure 6b** with 100 pulses at ~180 mJ cm^{-2}.

http://dx.doi.org/10.5772/66377

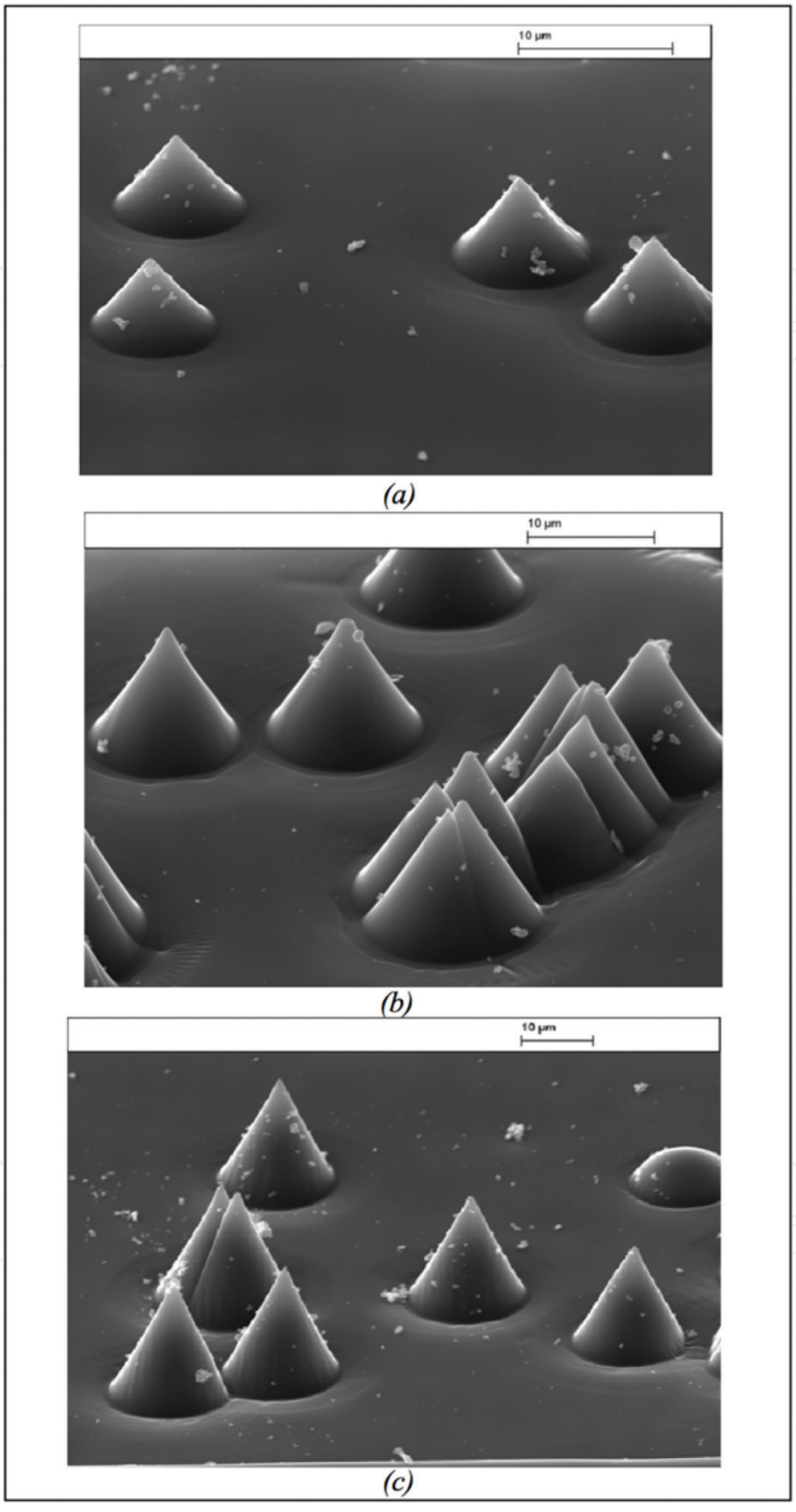

Figure 5. Evolution of conical structures developed on CR39 using the 157 nm laser (a) 500 pulses at ~80 mJ cm^{-2} (b) 500 pulses at ~112 mJ cm^{-2} (c) 500 pulses at ~140 mJ cm^{-2}.

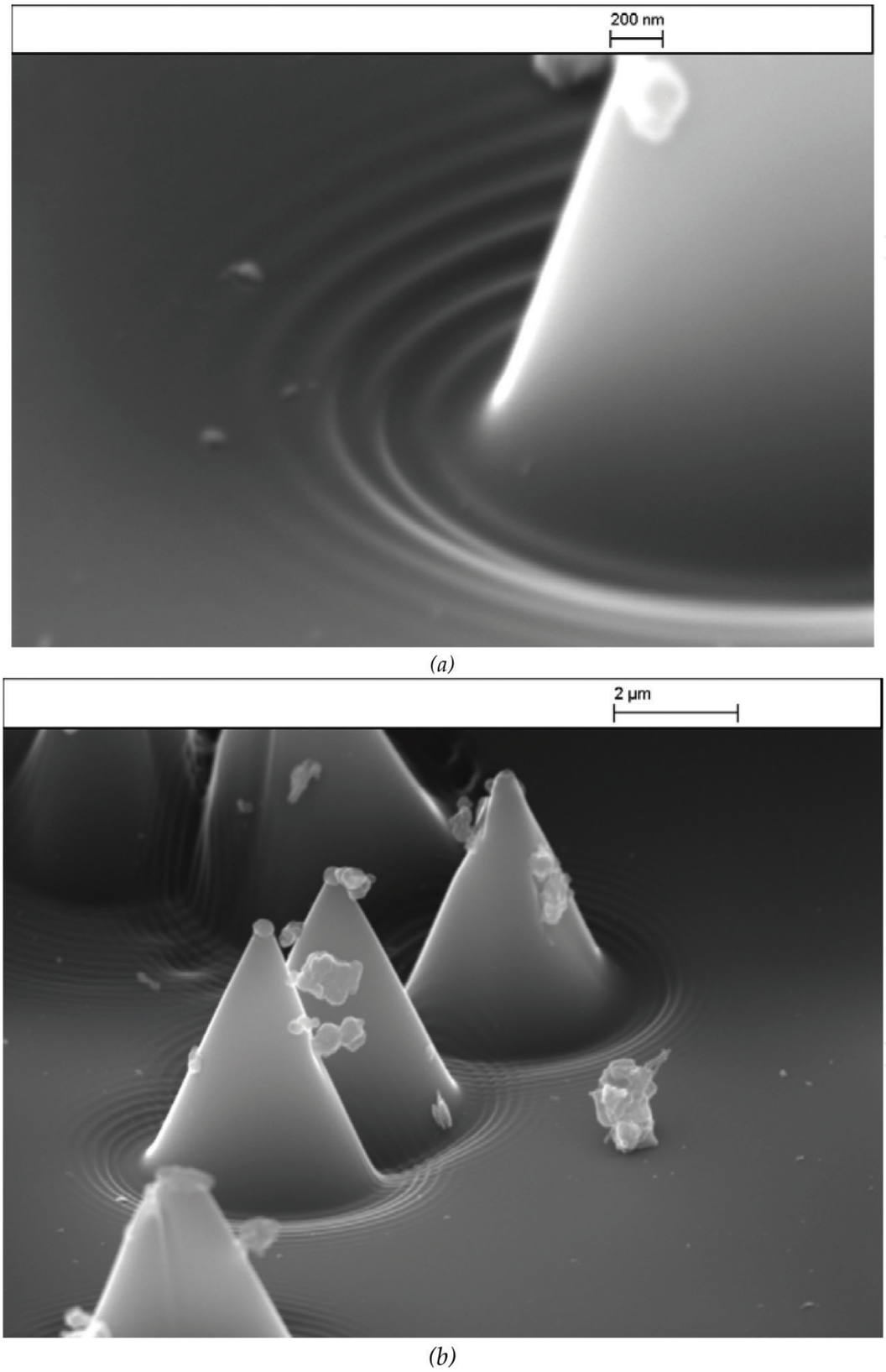

Figure 6. Fringes seen at the region of the bottom of the cones on CR39 (a) 100 pulses at ~60 mJ cm^{-2} and (b) 100 pulses at ~182 mJ cm^{-2}.

http://dx.doi.org/10.5772/66377

3.2. Pulsed UV laser at 248 nm

Figure 7 illustrates the microscopic image of the ablated CR39 craters spot size. The elimination of material and creation of the crater due to the ablation process are presented by the dark spot on the surface of the CR39. Partial transparent curves can be seen surrounding the edge of the craters. This could possibly be caused by the heat affected zone (HAZ), which occurs during the process of laser ablation. Heat affected zones (HAZ) are the outcome of materials that are molten due to heat transfer from the crater and then rapidly cooled. The short pulse width of the excimer laser nevertheless reduces the heat transfer from the ablated crater. This phenomenon is thought to be caused by the photothermal effect in which the laser energy absorption by the material is converted into heat energy, which in turn leads to the localized modification of its structure.

Figure 8 alternatively illustrates the average etch depth per pulse as a function of fluence F for CR39 ablated at 248 nm based on 150, 180, and 210 pulses. A linear fit of the form $d = k^{-1} \ln F/F_T$ provides an ablation threshold of 6–7 mJ cm^{-2}. This value is marginally lower than that reported using 157 nm laser which gives F_T as 11 mJ cm^{-2} [10].

3.3. Continuous UV laser at 244 nm

This section describes the use of this particular polymer as a waveguide where here we utilized a CR39 polymer sheet with a thickness of 0.5 mm and a refractive index as 1.486. Tunable laser

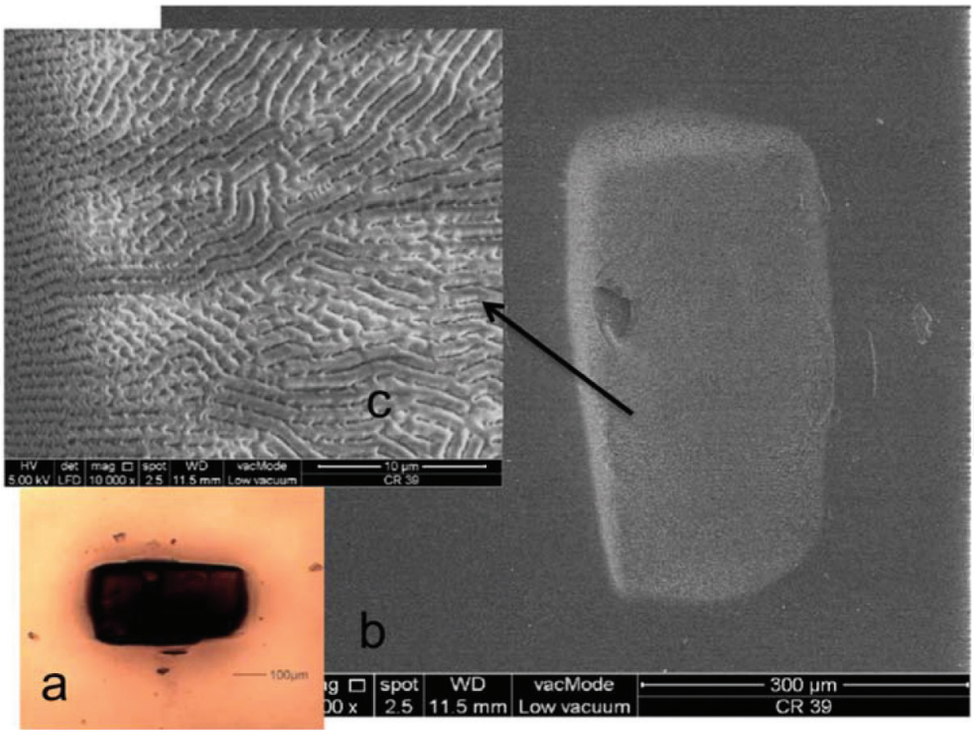

Figure 7. (a) Optical microscope imaging of the surface craters at CR39, (b) FESEM image of the crater, and (c) higher magnification of the ablated surface.

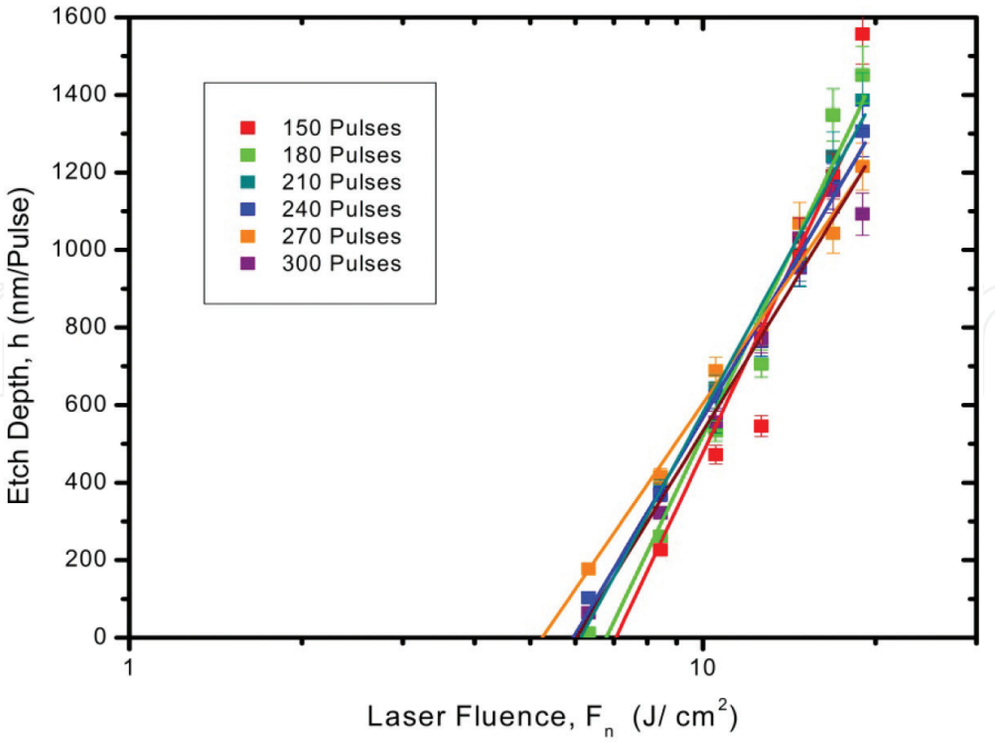

Figure 8. Plot of etch depth/pulse against log fluence at 150, 180, and 210 pulses on CR39.

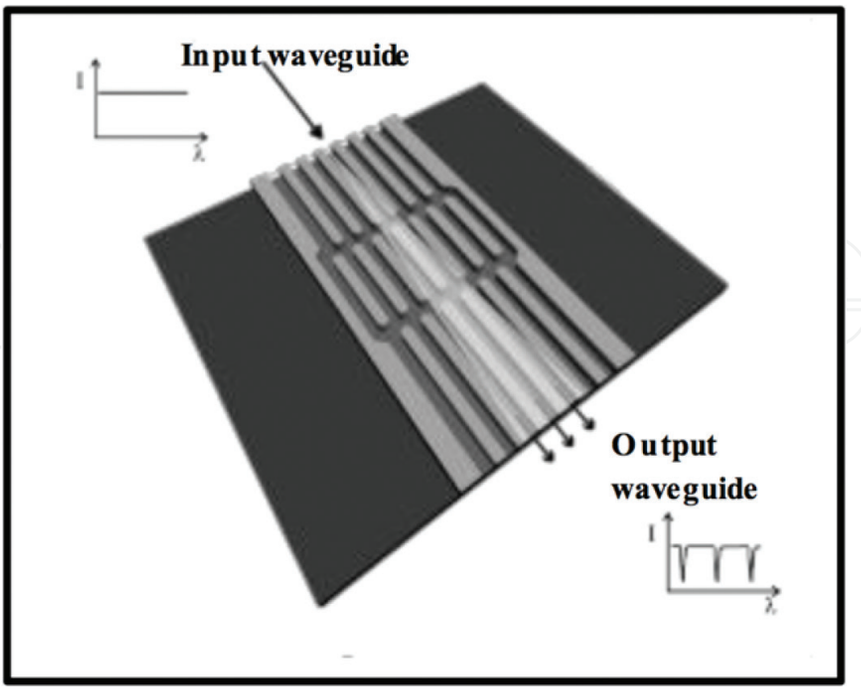

Figure 9. Optical waveguide channel fabricated on CR39.

http://dx.doi.org/10.5772/66377

source at 1550 nm (Sairon Technology SPA-4000 Prism Coupler) was used as a substrate for the polymer waveguide. SU-8 polymer was spin coated on the CR39 sheet and patterned using photolithography technique, formed a core of the channel waveguide structure. The height of the channel waveguide measured using optical microscopy was recorded as 5.0 ± 0.1 μm and width range between 10 and 15 μm. **Figure 9** shows the fabrication of the waveguide using photolithography technique.

Figure 10 shows the mode field diameter (MFD) and refractive index contrast of CR39 waveguide against the laser fluence. The refractive index change is seen to be more significant with the increase in fluence. Higher laser fluence will lead to a higher change of the refractive index, which likens to the reaction of other optical materials including silica glass to laser ablation. Extrapolation of the results in **Figure 10** also forecasts that the refractive index can be increased by the irradiation of CR39 with higher fluence. This increase, however, was observed to be limited as an upper fluence limit (5 KJ/cm^2) exists. When the laser fluence is above this limit, ablation will occur and subsequently UV irradiation of the CR39 will lead to the elimination of materials from its surface, similar to the outcome that occurs in Section 3.

The microscope image of the modification and ablation of CR39 is illustrated in **Figure 11**. As a result of refractive index modification, a partially transparent line can be seen in **Figure 11a**, whereas **Figure 11b** shows a darker line that indicates the removal of material and formation of craters due to ablation. The inset in **Figure 11b** further shows a cross-sectional view of the ablated sample. It is easier to detect the ablation effect from cross-sectional images in which a part of CR39 is removed. Subject to the laser fluence being applied, the removed area depth can be up to several microns.

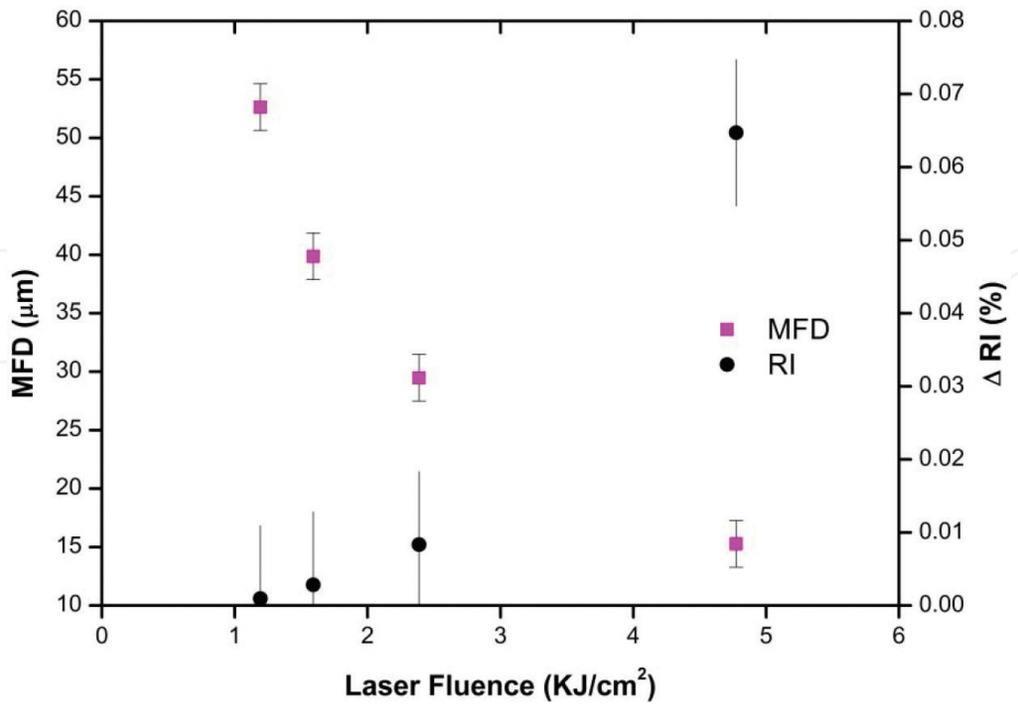

Figure 10. MFD and index contrast of CR39 waveguides versus laser fluence at 30 mW laser power.

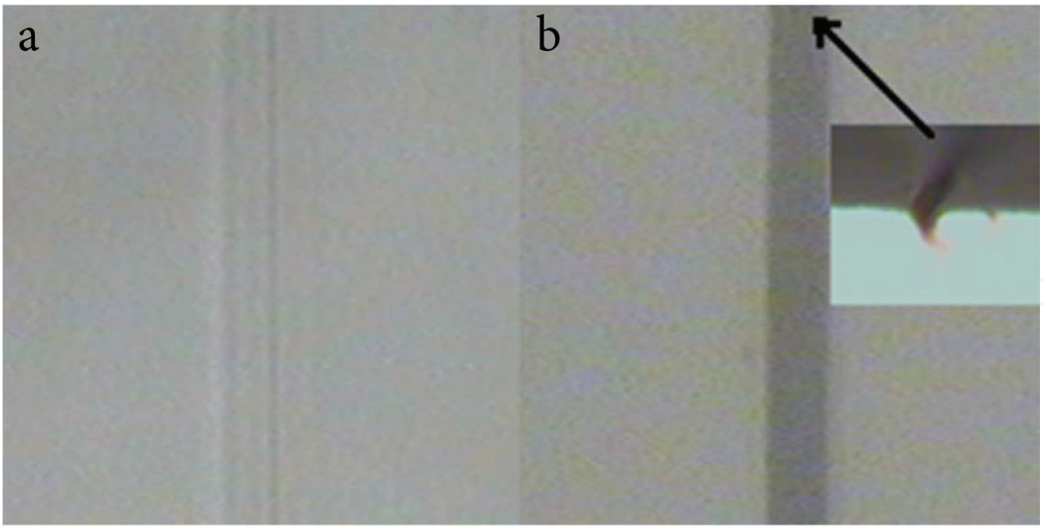

Figure 11. Microscope images of (a) internal modification, (b) ablation of CR39, and (inset) cross-sectional view of ablated CR39.

3.4. Application as optical waveguide

This section describes the use of laser process to fabricate optical waveguide that can be integrated into printed circuit board (PCB). Optical polymer materials offer a good aspect in terms of their relatively low cost and compatibility with traditional manufacturing process of PCB. Laser ablation is one of known approaches in processing PCB. The use of excimer laser has been repeatedly reported as it is capable of producing high-quality micromachining, which is sometimes ascribed as "cold ablation," which is possibly due to the UV absorption and the short pulse duration of the excimer laser.

Figure 12 shows the near-field image of one of the fabricated CR39 waveguides. The fabricated waveguides are observed to be faintly guided due to the light which is not well confined in the core, marked by the crosshair. The guiding characteristic of waveguide in which the largest refractive index variation measured is <0.07% for the range of fluence is verified as in **Figure 12**. It portrays that the fluctuations of refractive index caused by the laser fluence leads to a decrease in mode field diameter (MFD) due to better light confinement at the waveguide core.

The higher the variation of refractive index, the stronger the waveguides confinement in which a larger portion of light is being confined in the core and this in turn leads to the reduction in the MFD of the waveguides.

The successful direct writing of straight waveguides proves that a positive refractive index reaction of CR39 occurs when irradiated by 244 nm UV laser since refractive index for core must be greater than the surrounding for light guiding by the principle total internal reflection. The actual mechanism leading to the variation of the CR39 refractive index is yet to be determined. Nonetheless, we believe that it is caused by the photothermal effect in which the laser energy absorption by the material is converted into heat energy, which in turn leads to the localized modification of its structure and subsequently the refractive index. Nevertheless, further investigation on the origins of refractive index modification in CR39 is still being carried out.

http://dx.doi.org/10.5772/66377

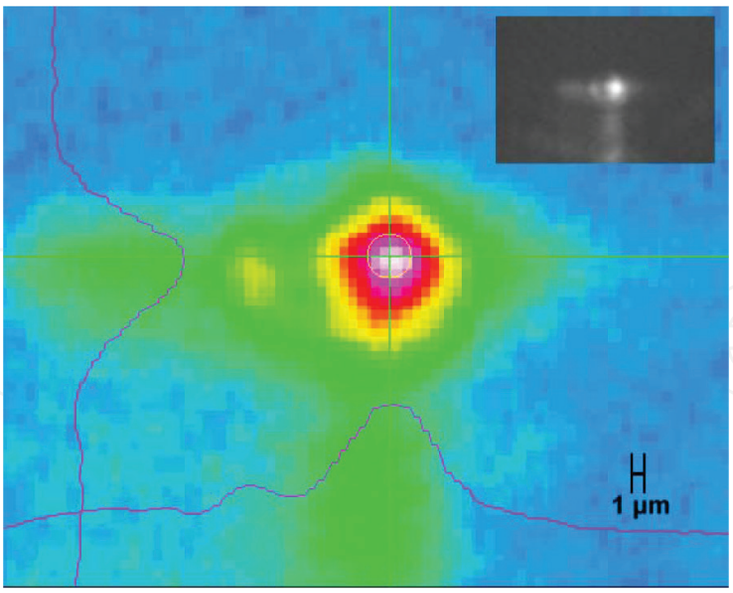

Figure 12. Near-field imaging of the CR39 waveguides.

4. Summary

This study deliberates the CR39 ablation with 248 nm UV laser. The variation in etch depth of craters is measured, and we can determine the fluence from the laser energy and spot size. There will be an increase in etch depth when the laser fluence is altered from 6.3 to 19.0 mJ cm^{-2}, respectively. Fluence threshold for CR39 is determined from the graph is 6 mJ cm^{-2}. Refractive index change from 1×10^{-5} to about 1×10^{-3} (0.0009–0.065%) is achieved on CR39 by varying the laser fluence from 1.2 to 4.8 KJ/cm^2, respectively. We suspect that the mechanism responsible for the refractive index change in CR39 by 244 nm laser irradiation is due to photothermal effect where localized heat generated by absorption of 244 nm laser modifies the structure/densified of CR39.

Author details

Rozalina Zakaria

Address all correspondence to: rozalina@um.edu.my

Photonics Research Centre, Faculty Science, University of Malaya, Kuala Lumpur, Malaysia

References

[1] Dyer, P.E., Excimer laser polymer ablation: twenty years on. Applied Physics A, 2003. 77(2): pp. 167–173.

[2] Jae-Hoon, L., et al., Enhanced extraction efficiency of ingan-based light-emitting diodes using 100-kHz femtosecond-laser-scribing technology. Electron Device Letters, IEEE, 2010. 31(3): pp. 213–215.

[3] Wu, C.-Y., Shu, C.-W., and Yeh, Z.-C., Effects of excimer laser illumination on microdrilling into an oblique polymer surface. Optics and Lasers in Engineering, 2006. 44(8): pp. 842–857.

[4] Lorenz, R.M., et al., Direct laser writing on electrolessly deposited thin metal films for applications in micro- and nanofluidics. Langmuir, 2004. 20(5): pp. 1833–1837.

[5] Cristea, D., et al., Polymer micromachining for micro- and nanophotonics. Materials Science and Engineering: C, 2006. 26(5–7): pp. 1049–1055.

[6] Cheng, Y., et al., Optical gratings embedded in photosensitive glass by photochemical reaction using a femtosecond laser. Optics Express, 2003. 11(15): pp. 1809–1816.

[7] Rafique, M.S., et al., Nonlinear absorption properties correlated with the surface and structural changes of ultra-short pulse laser irradiated CR-39. Applied Physics A, 2010. 100(4): pp. 1183–1189.

[8] Serafetinides, A.A., et al., Ultra-short pulsed laser ablation of polymers. Applied Surface Science, 2001. 180(1–2): pp. 42–56.

[9] Arshad K. Mairaj, et al., Fabrication and characterization of continuous wave direct UV (l= 244 nm) written channel waveguides in chalcogenide (Ga:La:S) glass. Journal of Lightwave Technology, 2002. 20(8).pp 1578–1584.

[10] Dyer, P.E., Walton, C.D., and Zakaria, R., Interference effects in 157 nm laser ablated cones in polycarbonate and application to spatial coherence measurement. Applied Physics A, 2009. 95: pp. 319–323.